Available online at www.sciencedirect.com

ScienceDirect

Current Opinion in Electrochemistry

Review Article

Methods and strategies for robust electrochemiluminescence signal quantification

Alessandro Fracassa[1], Chiara Mariani[1], Massimo Marcaccio[1], Guobao Xu[2,3], Neso Sojic[4], Giovanni Valenti[1] and Francesco Paolucci[1,5]

Abstract

Ever since the discovery of electrochemiluminescence (ECL), researchers have been devoted to exploring various approaches to improve the signal-to-noise ratio by testing different luminophores and introducing nanostructures, with the ultimate goal of enhancing analytical performance and expanding ECL's areas of application. In order to identify the most effective method and materials, the ECL quantum efficiency (ECL-QE) is the key parameter utilized for objective comparison among systems including different luminophores, co-reactants, electrode materials, experimental configurations, etc. However, due to the strong dependence of ECL on experimental parameters, developing an instrument-independent ECL-QE equation has proven challenging, resulting in significant variations in its value. Herein, we examine the most recent approaches for determining the ECL-QE in solution-phase and heterogeneous systems.

Addresses

[1] Dipartimento di Chimica "Ciamician", Università Degli Studi di Bologna, Via Selmi 2, 40126, Bologna, Italy
[2] State Key Laboratory of Electroanalytical Chemistry, Changchun Institute of Applied Chemistry, Chinese Academy of Sciences, 5625 Renmin Street, Changchun, Jilin, 130022, China
[3] University of Science and Technology of China, Hefei, 230026, China
[4] University of Bordeaux, Institut des Sciences Moléculaires, CNRS UMR 5255, 33607, Pessac, France
[5] CNR-ICMATE, Corso Stati Uniti 4, 35127 Padova, Italy

Corresponding authors: Paolucci, Francesco (francesco.paolucci@unibo.it); Valenti, Giovanni (g.valenti@unibo.it)

Current Opinion in Electrochemistry 2023, **41**:101375

This review comes from a themed issue on **Sensors and Biosensors (2023)**

Edited by **Dan Bizzotto** and **Thomas Doneux**

For complete overview about the section, refer Sensors and Biosensors (2023)

Available online 25 August 2023

https://doi.org/10.1016/j.coelec.2023.101375

Keywords:
Electrochemiluminescence, Quantum efficiency, Biosensors, Immunoassay, Coordination complexes.

Introduction

Electrochemiluminescence (ECL) has been a widely investigated phenomenon due to its advantageous applications in different fields, such as bioanalytical chemistry [1–3] and imaging [4–12]. The ECL emission is triggered by highly exergonic reactions among electrogenerated species, inducing the excitation of a given luminophore which ultimately emits light by relaxing to the ground state. The ECL process occurs via two main pathways, namely the annihilation and the co-reactant ones. The first mechanism is based on the homogeneous electron-transfer (eT) reaction between radical cations ($R^{\bullet+}$) and radical anions ($R^{\bullet-}$) which are generated at a single working electrode surface from a parent luminophore by applying an alternating potential [13–15]. The co-reactant pathway involves a luminophore and a sacrificial molecular species called co-reactant. The electrochemical system is swept up to a single and constant voltage value, limiting the working potential window just to the anodic or the cathodic region. Thus, the discovery of this approach by Bard and coworkers in the 80s overcame the obligation to carry out ECL in aprotic media, opening up the possibility for its generation in aqueous solution [16–18]. The co-reactant pathway is also viable in heterogeneous phase, where the luminophore is immobilized far from the electrode surface and cannot be directly oxidized. This is the case of ECL labels attached to immunoassays for clinical diagnosis or to living cell membranes for imaging. In heterogeneous phase, the luminophore must exhibit favorable electrochemical properties to engage in homogeneous redox reactions with electrogenerated co-reactant radicals, and suitable photophysical properties to achieve excitation [19].

In the ECL field, it is a popular approach to study different classes of luminophores for replacing the massively used $[Ru(bpy)_3]^{2+}$ in the attempt to pursue the quest for a better dye for improved signal-to-noise ratio. Prominent examples include Ir(III) complexes [20–27], molecular structures bearing multiple emitting units [28–30], nanomaterials [31,32], thermally activated delayed fluorescence (TADF) emitters [33–36].

In this context, quantum efficiency (QE) steps up as a crucial parameter that allows an objective comparison of a wide variety of luminophores under different experimental conditions. Within ECL, QE is defined as the ratio between the total number of photons generated from ECL processes and the total number of electrons injected into the system (ECL-QE).

Herein, we present novel approaches that provide a consistent quantification of the absolute ECL efficiency within a given chemical system. These methods offer the potential to build a comprehensive library for comparative purposes. The addressed strategies have been thoughtfully developed to be applicable in several experimental conditions: (i) annihilation ECL in aprotic solvents, which provide a wide potential stability window, (ii) co-reactant ECL where both the dye and the co-reactant are free to diffuse in solution (i.e., homogeneous configuration) and undergo redox processes through a single potential sweep and (iii) bead-based ECL immunoassay (i.e., heterogeneous configuration) where the luminophore is not free to diffuse to be directly transformed at the electrode surface.

Historical perspectives

Despite the acknowledged importance of the ECL, the literature lacks a widely accepted method for determining the ECL-QE whose value suffers from large variations, demonstrating the numerous difficulties in the measurement and reflecting differences in experimental procedures [37–41].

During the early-70s Faulkner's group proposed a novel experimental apparatus including an integrating sphere for performing ECL-QE measurements [42]. They also developed a mathematical model to describe the quantitative nature of ECL transient processes [43]. However, the integrating sphere is bulky, requires time-consuming calibration, the use of solutions free from impurities, and yields wavelength-dependent results. Furthermore, the mathematical framework requires a deep mechanistic knowledge of the system under examination. Anyway, a steady-state approach is preferable over a transient one where the solution conditions may vary between the first and the subsequent pulses due to the buildup of radicals and decomposition products near the electrode surface, as well as partial removal of quencher species (i.e., O_2) by radical ions or excited molecules.

Around the same time, Bard and coworkers introduced the possibility to perform ECL-QE experiments with a rotating ring-disc electrode (RRDE) to finally achieve steady-state ECL measurements. They computed ECL-QE via actinometry using a solution of potassium ferrioxalate $K_3[Fe(C_2O_4)_3]$ that was calibrated using a light-emitting surrogate of the RRDE [44]. Next, they calculated the ECL-QE of $[Ru(bpy)_3]^{2+}$ via RRDE experiments recording the ECL with a calibrated photodiode. They applied a novel system of corrections, including adjusting the total emission for the geometry factor, the reflectivity of the working electrode, the solution self-absorbance, and the relative area of the photodiode. They also fixed the recorded current for the residual signal [41,45–47]. Yet, corrections for these effects in luminescence measurement introduce the largest uncertainty due to their strong dependence on many experimental parameters, such as the solution photophysics, the cell configuration, and the losses from the insulating portions on the RRDE. Thus, instead of using very precise correction factors, they approximated them.

For their subsequent ECL-QE experiments on new electrochemical systems, Bard and colleagues established the well-known practice of reporting the QE relatively to that of 5% corresponding to $[Ru(bpy)_3]^{2+}$ in acetonitrile (ACN) following the annihilation mechanism which was determined in 1973 by Tokel et al. and is considered to be the "gold standard" [45,48–50].

Relative ECL-QE is determined by computing the following equation:

$$\Phi_{ECL,x} = \Phi_{ECL,st} \cdot \left(\frac{ECL_x}{ECL_{st}}\right) \cdot \left(\frac{Q_{st}}{Q_x}\right) \qquad (1)$$

where Φ_{ECL} represents the ECL-QE, ECL is the integrated signal, Q is the total injected charge expressed in Coulomb and *st* and *x* refer, respectively, to the standard $[Ru(bpy)_3]^{2+}$ and to the examined luminophore.

Clearly, this is not the best solution because the standard ECL-QE of 5% belonging to $[Ru(bpy)_3]^{2+}$ was retrieved at a specific luminophore concentration in a given solvent, with a given electrode material, at a well-defined RRDE rotation rate, and by considering approximated corrections. All these variables affect to a non-negligible extent the emission mechanism and the ECL performance of a particular system. Thus, relative ECL would be meaningless if different experimental conditions, compared to those of the standard, are employed. Nowadays, to address this limit, the most popular approach is to determine relative ECL-QE with respect to the efficiency of $[Ru(bpy)_3]^{2+}$, evaluated in the experimental conditions and by using the same instrumentation as for those employed for the considered luminophore *x*. Nonetheless, the adoption of different instruments among various laboratories makes it impossible to achieve reliable comparisons among diverse luminophores investigated by separate research groups.

In this context, several research groups have recently explored novel approaches for the determination of the absolute ECL-QE that is dependent only on the

chemistry of the system while independent from the instrumental apparatus and the experimental conditions.

Homogeneous ECL

ECL emission can occur via annihilation following the exergonic electron transfer between radical cations and radical anions (Scheme S1). Both species are generated from the parent luminophore at the electrode surface by pulsing potential steps of opposite polarity. Two essential parameters affect the ECL emission: the parent luminophore concentration and the potential pulsing frequency. The luminophore concentration usually ranges from 0.1 mM up to 5 mM. Generally, increasing the dye concentration correspondingly enhances the annihilation ECL signal. However, one must be aware about the Stokes shift of the considered emitter as it may lead to a signal underestimation. For most of the electrochemical cells, the ECL intensity increases as the pulsing frequency is raised within the range of 0.2−100 Hz. This is due to the generation of a greater amount of ECL reagents per unit time [46]. The pulsing frequency range can be pushed even further, up to 21 kHz by exploiting microelectrodes as the working one [51]. Past the upper frequency limit, the ECL intensity significantly drops off because the amount of time needed for charging the electrode to the desired potential is larger than the potential step duration imposed by the given frequency. In this way the radical ions generated on the previous step have a greater probability for diffusing away or being consumed by the electrode than reacting with each other. Thus, the magnitude of the cell time constant is critical in determining the upper frequency limit. However, the annihilation ECL is limited to fundamental studies since the generation of radical ions requires a wide electrochemical stability window typical of aprotic solvents such as ACN and tetrahydrofuran.

Alternatively, ECL can be produced with the aid of a co-reactant by sweeping the electrode to a single given potential. The most widely used luminophore and co-reactant are $[Ru(bpy)_3]^{2+}$ and tri-*n*-propylamine (TPrA), respectively. This system generates ECL via different pathways, contingent upon the applied potential and the concentration ratio between the two involved species. Among these mechanisms, the most important one involves the reaction of the oxidized $[Ru(bpy)_3]^{3+}$ [$E_{1/2}(Ru^{2+}/Ru^{3+}) = 1.05$ V in aqueous solution *vs* Ag/AgCl (3M NaCl)] [52] with the strongly reducing $TPrA^{\bullet}$ ($E_{ox} \approx -1.7$ V vs Ag/AgCl) [53] to yield the emitting $[Ru(bpy)_3]^{2+*}$ (Scheme S2.1). TPrA is firstly oxidized at the electrode surface to $TPrA^{\bullet+}$ [$E_{ox} = 0.83$ V in aqueous solution *vs* Ag/AgCl (saturated KCl)] that, in turn, undergoes facile deprotonation resulting in $TPrA^{\bullet}$ formation. Nevertheless, the oxidation rate of TPrA results to be sluggish due to the inner-sphere mechanism of heterogeneous electron transfer. Consequently, a substantial excess of co-reactant is usually employed to enhance the ECL emission. On the other hand, when the concentration ratio between $[Ru(bpy)_3]^{2+}$ and TPrA becomes comparable (e.g., differing by just one order of magnitude or less), the light-producing process travels down a parallel path, namely the "catalytic route", in which the oxidized $[Ru(bpy)_3]^{3+}$ promotes the homogeneous oxidation of TPrA (Scheme S2.2). This mechanism improves the concentration of $TPrA^{\bullet+}$ further from electrode surface, thereby extending the ECL-active layer. In this context, the concentration ratio between the dye and the co-reactant plays a pivotal role by tuning the thickness of the emitting layer and by forcing one of the two available pathways [54]. Instead, in the potential region where only the TPrA oxidation occurs, the "remote ECL" stands as the only active mechanism, in which $TPrA^{\bullet}$ reduces $[Ru(bpy)_3]^{2+}$ to $[Ru(bpy)_3]^{+}$ that is subsequently excited via eT with $TPrA^{\bullet+}$ (Scheme S2.3).

The potential necessary to trigger all of the mechanisms based on a co-reactant is not sufficiently anodic to evolve molecular oxygen, thus, aqueous solutions became a viable media for performing co-reactant ECL.

In this context, Ding and coworkers recently revisited the pioneering ideas on correction factors formulated by Bard and proposed a novel remarkable approach for calculating a corrected absolute annihilation ECL-QE and the first-ever absolute co-reactant ECL-QE by employing readily-available devices such as a photomultiplier tube (PMT), a photon counting head (PCH) and a charge-coupled device (CCD) camera [55−59].

PMT and PCH

As already mentioned, the absolute QE of an ECL system is defined as the ratio of the total number of photons emitted to the total number of electrons injected (Eq. (2)). To achieve instrument-independency, both quantities must be corrected by several correction factors and, eventually, the numerator and the denominator must be integrated with respect to the same time interval as follows:

$$\Phi_{ECL}(\%) = \frac{\int_0^t \nu_{photons}\, dt}{\int_0^t \nu_{electrons}\, dt} \times 100\% \qquad (2)$$

where $\nu_{photons}$ is the corrected total photon emission rate in units of photons • s^{-1}, while $\nu_{electrons}$ is the corrected total electron input expressed in electrons • s^{-1}. When a PMT is used as the photodetector, the outcome of an ECL measurement is a photocurrent (PC_{PMT}). The latter must account for multiple factors to yield $\nu_{photons}$ and, eventually, integrated over the entire duration of the experiment in the time domain, allowing for the determination of the total photon count (Eq. (3)).

$$\Phi_{ECL}^{PMT}(\%) = \frac{\int_0^t PC_{PMT} \times N_A \times (abs.\ correction\ factor)/_{F \times \sigma \times C}\ dt}{\int_0^t i \times (charge\ correction\ factor)/_{q_e}\ dt} \quad (3)$$

where N_A and F do not represent correction factors but the Avogadro number and the Faraday constant, respectively.

Conversely, the PCH photodetector works in single-photon counting mode, offering a direct quantification of the total photons generated during the ECL experiment (*total counts*) and neglecting the need for integration (Eq. (4)).

$$\Phi_{ECL}^{PCH}(\%) = \frac{(total\ counts) \times (abs.\ correction\ factor)/_{\sigma \times C}}{\int_0^t i \times (charge\ correction\ factor)/_{q_e}\ dt} \quad (4)$$

The *absorption correction factor* is a dimensionless correction that accounts for the eventual self-absorption effect that occurs when the emitting species exhibits a significant overlap between the absorption and emission spectra. They determined the magnitude of self-absorption by comparing the ECL spectrum to the absorption spectrum through a Gaussian fitting (e.g., 1.18 for $[Ru(bpy)_3]^{2+}$).

The dimensionless parameter σ expresses the total number of spheres of ECL emission and it is meant to correct the surface area of the photodetector while also considering the effect of electrode reflectivity. Basically, the light source is assumed to be a point one that emits isotropically in a spherical fashion [46]. However, only one hemisphere of emitted light will directly strike the detector while the other is projected toward the electrode surface that, in turn, will be partially reflected back. Ding and coworkers proposed a geometrical correction for switching from a planar detector surface to a spherical one. The latter surrounds the point source so that both hemispheres of emission are captured, thus the recorded signal should neglect the reflected light. Thus, the fraction of the light that is intercepted by the photodetector may be described using the following relationship:

$$\sigma = \frac{A_{detector}}{4\pi(d_{ECL\ to\ detector})^2}\ (1 + R_{elec}) \quad (5)$$

where $A_{detector}$ is the detector surface area, $4 \times \pi \times (d_{ECL\ to\ detector})^2$ is the total surface area of the ECL emission spheres created by the distance between the electrode surface and the PMT surface ($d_{ECL\ to\ detector}$) and R_{elec} is the reflectivity of the electrode material at the wavelength of maximum ECL emission. In general, a flat area can be converted in a spherical area while limiting the calculations error to less than 1%, when $d_{ECL\ to\ detector}$ ranges between 5 and 50 times the electrode diameter. This requirement is commonly referred to as the '5 times rule' [60].

The parameter C describes a hardware-specific, wavelength-specific correction factor which application is necessary to account for differences in hardware sensitivity to specific incoming light. This factor represents the average photodetector response to ECL emission in terms of electrons per incoming photon and it is computed as follows:

$$C = \frac{\int Q(\lambda) \times S(\lambda) \times d\lambda}{\int S(\lambda) \times d\lambda} \quad (6)$$

where $S(\lambda)$ is the background-subtracted, normalized emission spectrum of the ECL light while $Q(\lambda)$ is the calibrated QE of the photodetector. $Q(\lambda)$ is obtained by taking the manufacturer-provided $QE(\lambda)$ of the photodetector and multiplying it for a calibration factor (CC). The CC value is determined from the slope of a calibration line where the response of the photodetector itself toward the light emitted from a LED at different potentials is plotted against a photodiode response toward the same light. This calibration is roughly suitable for ±50 nm around the calibrated wavelength belonging to the LED emission.

On the other hand, it is also essential to apply a correction to the total number of injected electrons. In particular, the Faradaic current must be distinguished from the total measured current which includes also non-Faradaic processes that does not contribute to ECL emission. Ding and coworkers proposed the following charge correction factor:

$$charge\ correction\ factor = 1 - \frac{\int |i_{BG}| dt}{\int |i_x| dt} \quad (7)$$

where $|i_x|$ symbolizes the absolute current belonging to pulsing experiments while $|i_{BG}|$ represents the absolute background current determined by performing the same pulsing measurements but by applying potentials slightly below the oxidation or reduction threshold of the emitting species.

Eventually, in Eqs. (3) and (4), i is the current recorded during the ECL measurement, q_e is the electron elementary charge, and t is the total time interval of the ECL evaluation.

The conventional experimental apparatus for measuring the QE of homogeneous ECL by using either a PMT or PCH as the photodetector, is illustrated in Figure 1.

In one of their studies, Ding and colleagues conducted ECL-QE measurements in a homogeneous $[Ru(bpy)_3]^{2+}$/TPrA system to investigate the impact of the co-reactant concentration on the ECL-QE by steadily raising the amount of TPrA in solution while maintaining constant that of luminophore (Table 1) [56]. The ECL-QE determined from the co-reactant system at 1 mM $[Ru(bpy)_3]^{2+}$ and 10 mM TPrA displays a remarkable 3-fold enhancement compared to the efficiency observed for annihilating a 1 mM solution of $[Ru(bpy)_3]^{2+}$. This comparison highlights the significant role of TPrA that, beyond limiting the working potential window, is instrumental in enhancing the analytical performance of the ECL.

CCD device

Unfortunately, the ECL-QE measurements performed with a PMT or a PCH involve complex calibrations and poor sensitivity to unusual spectral regions. Recently, Ding and coworkers presented an instrumentally and mathematically simpler method for the ECL-QE determination (Eq. (8)). This novel approach employs a different experimental apparatus, including a spectrometer coupled to a spectroscopy CCD camera calibrated against a standardized photodiode (Figure 2) [59]. Generally, the calibration should be carried out once a year and unless the setup is modified, it should remain stable.

For this kind of device, the optical pathway for the emitted light from the electrode surface to the photodetector is quite different compared to the instrumentation previously presented and, thus, different correction factors must be considered:

$$\Phi_{ECL}(\%) = \frac{\int_0^t \sum_{pixel=1}^{pixel=w} \nu_{photons}\, dt}{\int_0^t \nu_{electrons}\, dt} \times 100\% = \frac{\int_0^t I_{corr} \times GF \times CC \times (abs.\ correction\ factor)_{/t} \times \sigma_{CCD}\, dt}{\int_0^t i \times (charge\ correction\ factor)_{/q_e}\, dt} \quad (8)$$

Figure 1

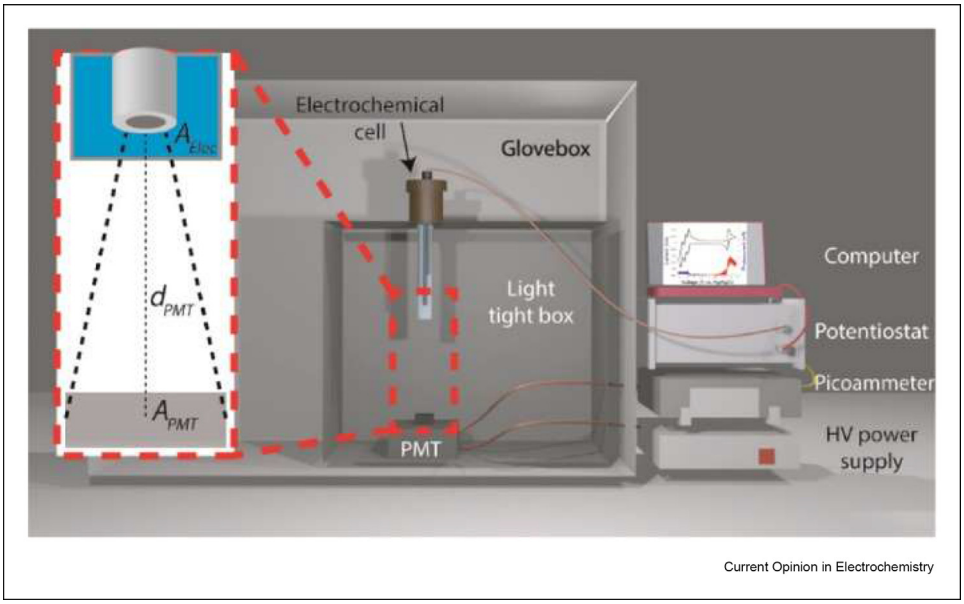

Conventional apparatus for ECL-QE measurements. The electrochemical cell is housed in a light tight box and includes a three-electrode setup. The working electrode (WE) is meticulously placed perpendicularly to the PMT photodetector, with precise consideration on the distance (d_{PMT}) to meet the criteria for the "5 times rule". The imposition of a potential step is performed by a potentiostat, while the resulting ECL output is collected as photocurrent by the PMT. In turn, the photocurrent is drawn by the picoammeter leading to a voltage drop across the terminals of its circuit. The voltage is ultimately translated into arbitrary units of emission through computational processing. The inset represents the solid angle of the ECL from the WE to the PMT (adapted with permission from Adsetts et al. [55] Copyright 2023 American Chemical Society).

Table 1

ECL-QE values obtained from PCH-recorded ECL signals in annihilation and in $[Ru(bpy)_3]^{2+}$/TPrA systems. $Ru(bpy)_3(PF_6)_2$ concentration was 1 mM for all experiments that are carried out in acetonitrile with 0.1 M $TBAPF_6$ as supporting electrolyte. Every experiment was repeated at least three times. Errors provided represent the standard deviation calculated across individual measurements. The annihilation experiments were performed by stepping the applied potential between 1.35 and –1.36 V vs. SCE while the co-reactant experiments were carried out between 0 and 1.5 V vs SCE (adapted with permission from Chu et al. [56] Copyright 2023 American Chemical Society.

	Cyclic voltammetry (%)	Pulsing stepping (10 Hz) (%)
Annihilation	0.0033 ± 0.0011	3.2 ± 0.1
5 mM TPrA	1.5 ± 0.3	7.5 ± 1.2
10 mM TPrA	3.1 ± 0.7	10.0 ± 1.1
20 mM TPrA	1.8 ± 0.4	2.0 ± 0.3
50 mM TPrA	0.8 ± 0.1	0.5 ± 0.2

where $\nu_{photons}$ is the corrected total photon emission rate on a pixel in units of photons • s^{-1}, $\Sigma\nu_{photons}$ is the sum of all photons in a defined pixel range and w is the width of the pixel array, while $\nu_{electrons}$ is the corrected total electron input in electrons • s^{-1} and is calculated as previously discussed.

Figure 2

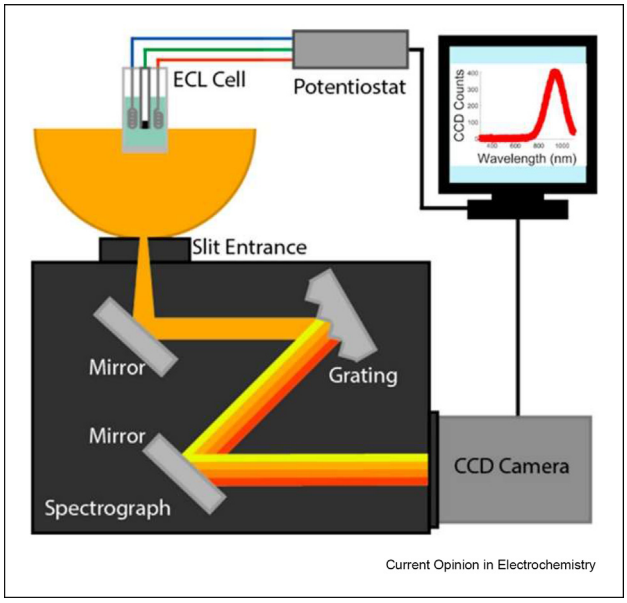

Experimental setup for QE measurements, employing a CCD camera as the photodetector coupled with a spectrograph. The electrochemical workstation includes a potentiostat connected with both the computer and the ECL cell featuring a three-electrode setup. Notably, the ECL emission does not strikes directly the photodetector but follows a complex pathway, that is defined by the spectrometer components, before ultimately reaching the CCD camera (adapted with permission from Adsetts et al. [59] Copyright 2023 American Chemical Society).

I_{corr} represents the emission intensity corrected for the wavelength-dependent transmission spectrum of the cell glass $Q(\lambda)$ and it is determined by dividing the crude number of counts I by $Q(\lambda)$:

$$I_{corr} = \frac{I}{Q(\lambda)} \tag{9}$$

GF is the gain factor provided by the manufacturer for a given CCD camera, CC is the aforementioned calibration factor, the *absorption correction factor* accounts for the self-absorption effect and it is computed as described above, and t is the accumulation time for the experiment.

Finally, σ_{CCD} represents the correction for the reflectivity and the solid angle of emission that is required since the spectrometer slit allows only a small portion of the total ECL emission to enter. σ_{CCD} is expressed according to the equation:

$$\sigma_{CCD} = \frac{A}{4\pi \times d^2} \times (1 + R_{elec}) \tag{10}$$

where A is the surface area of the slit while d is the distance between the electrode surface and the spectrometer slit and R_{elec} is the electrode reflectivity.

However, in most ECL-generating systems, a significantly higher concentration of TPrA is required compared to that of $[Ru(bpy)_3]^{2+}$, mainly to overcome the slow kinetics of heterogeneous electron transfer associated to the co-reactant. The current produced during the anodic potential sweep in such systems is predominantly driven by the oxidation of TPrA. As a result, distinguishing between the current contributions from TPrA and $[Ru(bpy)_3]^{2+}$ oxidations is considerably challenging. While the addition of a minute amount of $[Ru(bpy)_3]^{2+}$ can enhance ECL emission under these circumstances, it does not result in a proportional increase in the recorded current.

Finite element simulation

The aforementioned approaches require accurate experimental control, deep knowledge of instrumentation, and careful data handling as multiple instrument-dependent correction factors must be introduced to achieve accurate ECL-QE measurements. Furthermore, it is not easy to quantify the exact current generated by $[Ru(bpy)_3]^{2+}$ in a system containing a high concentration of co-reactant.

In principle, QE can be expressed as the product between the efficiency of electrochemical excitation (η_{ex}) and the photoluminescence quantum yield (PLQY). Given the PLQY of $[Ru(bpy)_3]^{2+}$ to be 4.2%, the ECL-QE is virtually determined by η_{ex}, which was computed for the $[Ru(bpy)_3]^{2+}$/TPrA system by Bin S. et al. using finite element simulation [61].

The upper limit imposed by the PLQY can be approached on the glassy carbon (GC) working electrode (WE) at a concentration ratio [TPrA]/[$Ru(bpy)_3^{2+}$] of 200 while this optimal ratio is increased, respectively, to 1000 and 4000 on Pt and indium tin oxide (ITO) working electrodes. This trend can be explained with the gradually slower oxidation rate of TPrA which can be balanced with a higher concentration of co-reactant.

Simulating the electrochemical system at different WE potentials (from 1.10 V to 1.25 V) yields interesting results as well. In fact, on a GC WE, an increase in applied potential does not affect the QE at a [TPrA]/[$Ru(bpy)_3^{2+}$] ratio of 1000, which remains constant for several μm from the electrode surface, while it slightly decreases at a concentration ratio of 10. This result can be explained by the oxidative dissipation of $TPrA^{\bullet}$ (Reactions S2.1.7, S2.2.8, S2.3.6) which is already produced in a good amount at smaller overpotentials. The Pt WE presents a very similar situation at concentration ratio of 1000 but, when the latter drops to 100, increasing the anodic voltage slightly increases the QE. Instead, at the ITO WE, QE is enhanced by pushing the voltage to more positive values in both situations of concentration ratio, namely 1000 and 100. The enhancement is explained with the improved oxidation rate of the co-reactant at higher overpotentials.

Additionally, according to their findings, the "catalytic route" emerges as a limiting factor for the ECL-QE. By increasing the initial [$Ru(bpy)_3^{2+}$]/[TPrA] ratio, the consumption of electrogenerated $[Ru(bpy)_3]^{3+}$ by homogeneous oxidation of TPrA to $TPrA^{\bullet+}$ becomes gradually more likely to occur with respect to the eT with $TPrA^{\bullet}$ that generates the emitting $[Ru(bpy)_3]^{2+*}$. In other words, by following the catalytic mechanism, the withdrawal of an electron from the luminophore does not translate in the generation of the excited state and, in turn, of a photon. The authors explored how the ECL-QE is affected by varying the rate constant of the 'catalytic route' at different ratio of k_1/k_2, where k_1 is the heterogeneous oxidation rate of $[Ru(bpy)_3]^{2+}$ while k_2 represents the heterogeneous oxidation rate of TPrA. It is interesting to note that at low values of k_1/k_2 the 'catalytic route' reaction rate barely affects QE. Instead, when $k_1 >> k_2$, the reaction rate plays a pivotal role, highlighting the importance of having a much higher starting concentration of TPrA in order to have more co-reactant molecules available for the oxidation process.

ECL-QE in heterogeneous system

Heterogeneous phase ECL finds extensive application in clinical diagnostic and imaging, where $[Ru(bpy)_3]^{2+}$ labels are attached to objects (i.e., magnetic beads or living cells) that constrict the luminophore labels far from the electrode surface. Thus, the only available light emitting mechanism is the 'remote (or heterogeneous) ECL' wherein the most efficient co-reactant is TPrA. Within heterogeneous ECL it is common practice to work in great excess of TPrA, usually 180 mM in a buffer solution. This ensures the ECL signal to be proportional to the luminophore loading, remaining unaffected from the co-reactant consumption.

Unfortunately, this reaction mechanism still faces several limitations. The kinetics of heterogeneous oxidation of TPrA is sluggish, and the poor stability of the oxidizing $TPrA^{\bullet+}$ confines the ECL emitting layer to a ~3 μm distance from the electrode surface. Moreover, the $[Ru(bpy)_3]^{2+}$ loading is limited by the surface area of the capturing object. To circumvent these problems, various strategies have been exploited, such as the introduction of nanostructures embedding multiple emitting units instead of single ECL labels [30], conductive carbon- and metal-based nanomaterials to tune the electroactive surface [62,63], water-soluble redox mediators [7], and beads of different dimensions to control the localization of Ru(II) labels at different distances from the electrode surface [64]. All the aforementioned approaches influence the ECL emission either by increasing the $[Ru(bpy)_3]^{2+}$ loading or by modifying specific steps of the reaction mechanism. On top of that, the oxidative-reduction heterogeneous mechanism is solely based on the oxidation of TPrA, making it difficult for the ECL-QE equation to account for the amount of $[Ru(bpy)_3]^{2+}$. Thus, it is desirable to rely on an equation that is normalized over the number of luminophore units, providing a measure of the efficiency of the reaction mechanism rather than focusing on the mere ECL emission.

To achieve that, Zanut and colleagues proposed the turnover frequency (TOF) as an appropriate parameter that offers a comprehensive assessment that considers both the efficiency of the light-generating mechanism and the intrinsic emission quantum yield of the dye. TOF is defined as the number of photons generated by a single luminophore in 1 s and calculated as follows:

$$\mathrm{TOF} = \frac{(\mathrm{ECL_{Ru@Bead}} - \mathrm{ECL_{Bead}})}{\mathrm{n^o of}\ \left[\mathrm{Ru(bpy)_3}\right]^{2+} \times \mathrm{time}} \qquad (11)$$

where $ECL_{Ru@Bead}$ is the integrated ECL signal of a given capturing object, a $[Ru(bpy)_3]^{2+}$-functionalized bead in this case, while ECL_{bead} represents the integrated ECL signal of a single unlabeled bead. Instead, n^o *of* $[Ru(bpy)_3]^{2+}$ represents the amount of Ru(II) labels on the functionalized bead, that is quantified either via inductively coupled plasma mass spectrometry (ICP-MS) after sample mineralization or via confocal microscopy. In this context, the ECL signal quantification become very challenging because the emission intensity strongly depends on the spatial distribution of the dye [6]. Therefore, TOF determination is carried out by exploiting ECL microscopy that provides outstanding spatial resolution and enables the observation of single objects [4].

This approach is intended to evaluate the stability of the dye together with its accessibility to the co-reactant radicals. In this way, the TOF enable the comparison between ECL systems under different experimental conditions and carrying different loadings of luminophore.

This strategy was applied for the very first time by Zanut et al. to determine the impact of bead size on the efficiency of the heterogeneous ECL mechanism (Figure 3a) [64]. Specifically, they investigated the emission of ruthenium-containing biotinylated antibodies linked to streptavidin beads of varying sizes: 2.8, 1, 0.5, and 0.3 μm. They discovered that the highest TOF was achieved with 0.3 μm beads, which were proved to be the most efficient (Figure 3b). The smallest beads express a larger surface area in close proximity to the electrode surface, leading to a greater concentration of $[Ru(bpy)_3]^{2+}$ within that region, where an active N-centered radical provides a parallel and more efficient ECL mechanism.

The same researchers subsequently employed the same strategy to investigate the ECL performances of Ru(II)-functionalized carbon nanotubes (CNTs) attached to 2.8 μm beads (Beads@CNT-Ru) [62]. The ECL signal integration of Beads@CNT-Ru resulted in a 1.7-fold TOF enhancement compared to the emission displayed by 2.8 μm beads directly linked to $[Ru(bpy)_3]^{2+}$ labels (Beads@Ru). This finding provides evidence of the strategic role played by CNTs which likely form a conductive electrocatalytic network randomly distributed on the beads. This carbonaceous arrangement enables the direct oxidation of TPrA at the beads surface, increasing the radicals concentration all around the microspheres.

However, TOF equation does not consider the injected electrons and the ECL optical pathway from the WE to the digital camera. Thus, in the interest of comparison, it would be beneficial to normalize TOF against the oxidation rate of the co-reactant and to introduce appropriate instrumental corrections.

Conclusion

While calculating the relative ECL-QE is simple and time-efficient, its comparability is hindered by variations in experimental equipment among different laboratories and the challenges operators face in replicating a given setup precisely. Conversely, the previously proposed strategies for determination of absolute ECL-QE either required complex instrumentation or lacked accuracy. Decades of fragmented literature on the determination of ECL-QE makes it impossible to confront the efficiency of different chemical systems. In this regard, researchers have recently made significant advancements by developing novel equations to achieve instrument-independent ECL-QE, paving the way for more reliable and comparable measurements. The solution-phase ECL-QE is

Figure 3

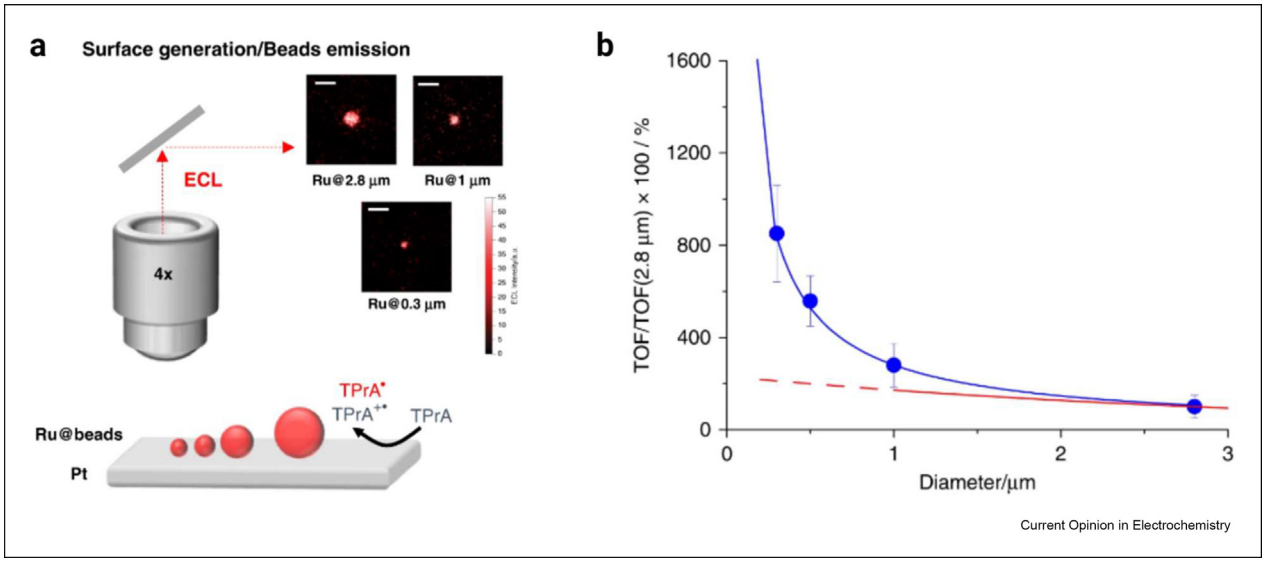

a) Schematic representation of the ECL microscopy experiment on single beads where Ru@beads stands for magnetic beads labeled with $[Ru(bpy)_3]^{2+}$ on a platinum electrode (Pt). The inset shows the ECL images aquired for beads with different sizes where *Ru@2.8* μm, Ru@1 μm and *Ru@0.3* μm are ECL images of $[Ru(bpy)_3]^{2+}$-labeled magnetic beads with a diameter of 2.8, 1 and 0.3 μm, respectively. Magnification 100×, Scale bar 5 μm; potential applied, 1.4 V (vs. Ag/AgCl, 3 M KCl); acquisition time 0.5 s. b) turnover frequency (TOF) as a function of bead size (blue curve and dots) and ECL intensity from Ref. [53] (red curve), both as functions of the beads size. The TOF values are normalized over *TOF@2.8* μm which is the turnover frequency for 2.8 μm beads (*Ru@2.8* μm) (reproduced from Zanut et al. [64] under Creative Commons Attribution 4.0 International License from Springer Nature). (For interpretation of the references to color/colour in this figure legend, the reader is referred to the Web version of this article.)

determined experimentally using readily-available instruments, with correction factors applied to account for the optical pathway of the ECL signal. Alternatively, a kinetic finite element simulation has been developed to overcome challenges such as the uncertainty on the attribution of the current intensity in co-reactant excess conditions and complex data elaboration. Additionally, the concept of TOF has been utilized to determine ECL-QE for heterogeneous systems, where the luminophore cannot be directly oxidized at the electrode surface. This allows for a rational evaluation of the mechanism efficiency over the intensity of total emission. Despite these advancements, the equations discussed in this opinion exhibit limitations that require further research to introduce other correction factors for making ECL-QE dependent solely on the chemistry of the system under exam. The creation of a comprehensive library of ECL-QE values would be invaluable for identifying the most effective enhancement strategies.

Declaration of competing interest

The authors declare the following financial interests/personal relationships that may be considered as potential competing interests: Francesco Paolucci reports financial support was provided by University of Bologna. Giovanni Valenti reports financial support was provided by European Commission.

Data availability

No data was used for the research described in the article.

Acknowledgments

This research was funded by MIUR, grant number 2017PBXPN4, 2017FJCPEX and 2020CBEYHC (AStraLI). This work was supported by ECLipse project that has received funding from the European Union's Horizon Europe EIC Pathfinder Open programme under Grant Agreement No 101046787. GV and FP would like to thank the NanoImmunoEra project. Nano-ImmunoEra project has received funding from the European Union's MSCA Staff exchange Horizon Europe programme Grant Agreement Number 101086341. N.S. acknowledges the financial support from ANR (ELISE - ANR-21-CE42-0008-01). G.X. and N.S. thank the Sino-French International Research Network ELECTROSENS (CNRS) and CAS President's International Fellowship Initiative (PIFI) for their financial support.

Appendix A. Supplementary data

Supplementary data to this article can be found online at https://doi.org/10.1016/j.coelec.2023.101375.

References

Papers of particular interest, published within the period of review, have been highlighted as:

* of special interest
** of outstanding interest

1. Sornambigai M, Bouffier L, Sojic N, Kumar SS: **Tris(2,2'-bipyridyl)ruthenium (II) complex as a universal reagent for the fabrication of heterogeneous electrochemiluminescence platforms and its recent analytical applications**. *Anal Bioanal Chem* 2023:1–24.

2. Du F, Chen Y, Meng C, Lou B, Zhang W, Xu G: **Recent advances in electrochemiluminescence immunoassay based on multiple-signal strategy**. *Curr Opin Electrochem* 2021, **28**, 100725.

3. Du F, Dong Z, Guan Y, Zeid AM, Ma D, Feng J, Yang D, Xu G: **Single-electrode electrochemical system for the visual and high-throughput electrochemiluminescence immunoassay**. *Anal Chem* 2022, **94**:2189–2194.

4. Rebeccani S, Zanut A, Santo CI, Valenti G, Paolucci F: **A guide inside electrochemiluminescent microscopy mechanisms for analytical performance improvement**. *Anal Chem* 2022, **94**: 336–348.

5. * Sentic M, Milutinovic M, Kanoufi F, Manojlovic D, Arbault S, Sojic N: **Mapping electrogenerated chemiluminescence reactivity in space: mechanistic insight into model systems used in immunoassays**. *Chem Sci* 2014, **5**:2568–2572.
For the first time, the authors investigated the remote ECL mechanism mechanisms of the reaction of the $[Ru(bpy)_3]^{2+}$ luminophore with two efficient co-reactants (TPrA or DBAE) via ECL microscopy by mapping the ECL reactivity at the level of single $[Ru(bpy)_3]^{2+}$-functionalized beads.

6. Fiorani A, Han D, Jiang D, Fang D, Paolucci F, Sojic N, Valenti G: **Spatially resolved electrochemiluminescence through a chemical lens**. *Chem Sci* 2020, **11**:10496–10500.

7. Kerr E, Knezevic S, Francis PS, Hogan CF, Valenti G, Paolucci F, Kanoufi F, Sojic N: **Electrochemiluminescence amplification in bead-based assays induced by a freely diffusing iridium(III) complex**. *ACS Sens* 2023, **8**:933–939.

8. Ding H, Guo W, Su B: **Imaging cell-matrix adhesions and collective migration of living cells by electrochemiluminescence microscopy**. *Angew Chem Int Ed* 2020, **59**:449–456.

9. Knežević S, Kerr E, Goudeau B, Valenti G, Paolucci F, Francis PS, Kanoufi F, Sojic N: **Bimodal electrochemiluminescence microscopy of single cells**. *Anal Chem* 2023, **95**:7372–7378.

10. Chen Y, Zhao D, Fu J, Gou X, Jiang D, Dong H, Zhu JJ: **In situ imaging facet-induced spatial heterogeneity of electrocatalytic reaction activity at the subparticle level via electrochemiluminescence microscopy**. *Anal Chem* 2019, **91**: 6829–6835.

11. Dong J, Xu Y, Zhang Z, Feng J: **Operando imaging of chemical activity on gold plates with single-molecule electrochemiluminescence microscopy**. *Angew Chem Int Ed* 2022, **61**, e2022001.

12. Chen MM, Xu CH, Zhao W, Chen HY, Xu JJ: **Super-resolution electrogenerated chemiluminescence microscopy for single-nanocatalyst imaging**. *J Am Chem Soc* 2021, **143**: 18511–18518.

13. Dufford RT, Nightingale D: **Luminescence of grignard compounds in electric and magnetic fields, and related electrical phenomena**. *J Am Chem Soc* 1927, **49**:1858–1864.

14. Santhanam KSV, Bard AJ: **Chemiluminescence of electrogenerated 9,10-diphenylanthracene anion radical**. *J Am Chem Soc* 1965, **87**:139–140.

15. Tokel NE, Bard AJ: **Electrogenerated chemiluminescence. IX. Electrochemistry and emission from systems containing tris(2,2'-bipyridine)ruthenium(II) dichloride**. *J Am Chem Soc* 1972, **94**:2862–2863.

16. Rubinstein I, Bard AJ: **Electrogenerated chemiluminescence. 37. Aqueous ecl systems based on Ru(2,2'-bipyridine)32+ and oxalate or organic acids**. *J Am Chem Soc* 1981, **103**: 512–516.

17. White HS, Bard AJ: **Electrogenerated chemiluminescence. 41. Electrogenerated chemiluminescence and chemiluminescence of the Ru(2,2'-bpy)32+-S2O82- system in acetonitrile-water solution**. *J Am Chem Soc* 1982, **104**: 6891–6895.

18. Noffsinger JB, Danielson ND: **Generation of chemiluminescence upon reaction of aliphatic amines with tris(2,2'-bipyridine) ruthenium(III)**. *Anal Chem* 1987, **59**:865–868.

19. Kerr E, Doeven EH, Wilson DJD, Hogan CF, Francis PS: **Considering the chemical energy requirements of the tri-n-propylamine co-reactant pathways for the judicious design of new electrogenerated chemiluminescence detection systems**. *Analyst* 2016, **141**:62–69.

20. Truong J, Spilstead KB, Barbante GJ, Doeven EH, Wilson DJD, Barnett NW, Henderson LC, Altimari JM, Hockey SC, Zhou M, Francis PS: **Chemiluminescence detection with water-soluble iridium(III) complexes containing a sulfonate-functionalised ancillary ligand**. *Analyst* 2014, **139**:6028–6035.

21. Barbante GJ, Doeven EH, Kerr E, Connell TU, Donnelly PS, White JM, Lópes T, Laird S, Wilson DJD, Barnard PJ, Hogan CF, Francis PS: **Understanding electrogenerated chemiluminescence efficiency in blue-shifted iridium(III)-complexes: an experimental and theoretical study**. *Chem Eur J* 2014, **20**:3322–3332.

22. Longhi E, Fernandez-Hernandez JM, Iordache A, Fröhlich R, Josel HP, De Cola L: **Ir(III) cyclometalated complexes containing phenylphenanthridine ligands with different substitutions: effects on the electrochemiluminescence properties**. *Inorg Chem* 2020, **59**:7435–7443.

23. Fernandez-Hernandez JM, Longhi E, Cysewski R, Polo F, Josel HP, De Cola L: **Photophysics and electrochemiluminescence of bright cyclometalated Ir(III) complexes in aqueous solutions**. *Anal Chem* 2016, **88**:4174–4178.

24. Chen L, Hayne DJ, Doeven EH, Agugiaro J, Wilson DJD, Henderson LC, Connell TU, Nai YH, Alexander R, Carrara S, Hogan CF, Donnelly PS, Francis PS: **A conceptual framework for the development of iridium(iii) complex-based electrogenerated chemiluminescence labels**. *Chem Sci* 2019, **10**:8654–8667.

25. Kerr E, Doeven EH, Barbante GJ, Connell TU, Donnelly PS, Wilson DJD, Ashton TD, Pfeffer FM, Francis PS: **Blue electrogenerated chemiluminescence from water-soluble iridium complexes containing sulfonated phenylpyridine or tetraethylene glycol derivatized triazolylpyridine ligands**. *Chem Eur J* 2015, **21**:14987–14995.

26. Newman B, Chen L, Henderson LC, Doeven EH, Francis PS, Hayne DJ: **Water-soluble iridium(III) complexes containing tetraethylene-glycol-derivatized bipyridine ligands for electrogenerated chemiluminescence detection**. *Front Chem* 2020, **8**, 583631.

27. Smith ZM, Kerr E, Doeven EH, Connell TU, Barnett NW, Donnelly PS, Haswell SJ, Francis PS: **Analytically useful blue chemiluminescence from a water-soluble iridium(iii) complex containing a tetraethylene glycol functionalised triazolylpyridine ligand**. *Analyst* 2016, **141**:2140–2144.

28. Fealy RJ, Goldsmith JI: **Investigating electron transfer in macromolecular ruthenium tris(bipyridyl) complexes using collection experiments at a rotating ring-disk electrode**. *J Phys Chem C* 2012, **116**:13133–13142.

29. Valenti G, Fiorani A, Di Motta S, Bergamini G, Gingras M, Ceroni P, Negri F, Paolucci F, Marcaccio M: **Molecular size and electronic structure combined effects on the electrogenerated chemiluminescence of sulfurated pyrene-cored dendrimers**. *Chem Eur J* 2015, **21**:2936–2947.

30. Zanut A, Palomba F, Rossi Scota M, Rebeccani S, Marcaccio M, Genovese D, Rampazzo E, Valenti G, Paolucci F, Prodi L: **Dye-doped silica nanoparticles for enhanced ECL-based immunoassay analytical performance**. *Angew Chem Int Ed* 2020, **59**:21858–21863.

31. Carrara S, Arcudi F, Prato M, De Cola L: **Amine-rich nitrogen-doped carbon nanodots as a platform for self-enhancing electrochemiluminescence**. *Angew Chem Int Ed* 2017, **56**:4757–4761.

32. Arcudi F, Đorđević L, Rebeccani S, Cacioppo M, Zanut A, Valenti G, Paolucci F, Prato M: **Lighting up the electrochemiluminescence of carbon dots through pre- and post-synthetic design**. *Adv Sci* 2021, **8**:1–9.

33. Ishimatsu R, Matsunami S, Kasahara T, Mizuno J, Edura T, Adachi C, Nakano K, Imato T: **Electrogenerated chemiluminescence of donor-acceptor molecules with thermally activated delayed fluorescence**. *Angew Chem Int Ed* 2014, **53**:6993–6996.

34. Kudruk S, Villani E, Polo F, Lamping S, Körsgen M, Arlinghaus HF, Paolucci F, Ravoo BJ, Valenti G, Rizzo F: **Solid state electrochemiluminescence from homogeneous and patterned monolayers of bifunctional spirobifluorene**. *Chem Commun* 2018, **54**:4999–5002.

35. Luo Y, Zhao B, Zhang B, Lan Y, Chen L, Zhang Y, Bao Y, Niu L: **A scaffold of thermally activated delayed fluorescent polymer dots towards aqueous electrochemiluminescence and biosensing applications**. *Analyst* 2022, **147**:2442–2451.

36. Pavan G, Morgan L, Demitri N, Alberoni C, Scattolin T, Aliprandi A: **Highly efficient electrochemiluminescence from imidazole-based thermally activated delayed fluorescence emitters**. *Chem Eur J* 2023, e202301912.

37. Hercules DM: **Chemiluminescence from electron-transfer reactions**. *Acc Chem Res* 1969, **2**:301–307.

38. Schwartz PM, Blakeley RA, Robinson BB: **Efficiency of the electrochemiluminescent process**. *J Phys Chem* 1972, **76**:1868–1871.

39. Bezman R, Faulkner LR: **Mechanism of chemiluminescent electron-transfer reactions. V. Absolute measurements of rubrene luminescence in benzonitrile and N,N-dimethylformamide**. *J Am Chem Soc* 1972, **94**:6324–6330.

40. Pighin A: **Effect of solvents on the quantum efficiency of rubrene electrogenerated chemiluminescence**. *Can J Chem* 1973, **51**:3467–3472.

41. Cormier MJ, Hercules DM, Lee J: *Chemiluminescence and bioluminescence*. Springer Science; 1973.

42. Bezman R, Faulkner LR: **Construction and calibration of an apparatus for absolute measurement of total luminescence at low levels**. *Anal Chem* 1971, **43**:1749–1753.

43. Bezman R, Faulkner LR: **Theoretical and practical considerations for measurements of the efficiencies of chemiluminescent electron-transfer reactions**. *J Am Chem Soc* 1972, **94**:3699–3707.

44. Maloy JT, Bard AJ: **Electrogenerated chemiluminescence. VI. Efficiency and mechanisms of 9,10-diphenylanthracene, rubrene, and pyrene systems at a rotating-ring-disk electrode**. *J Am Chem Soc* 1971, **93**:5968–5981.

45. Tokel NE, E HR, Bard AJ: **Electrogenerated chemiluminescence. XIII. Electrochemical and electrogenerated chemiluminescence studies of ruthenium chelates**. *J Am Chem Soc* 1973, **95**:6582–6589.

46. Keszthelyi CP, Tokel-Takvoryan NE, Bard AJ: **Electrogenerated chemiluminescence: determination of the absolute luminescence efficiency in electrogenerated chemiluminescence; 9,10-diphenylanthracene-thianthrene and other systems**. *Anal Chem* 1975, **47**:249–256.

47. Mussell RD, Nocera DG: **Effect of long-distance electron transfer on chemiluminescence efficiencies**. *J Am Chem Soc* 1988, **110**:2764–2772.

48. Wallace WL, Bard AJ: **Electrogenerated chemiluminescence. 35. Temperature dependence of the ECL efficiency of Ru(bpy)32+ in acetonitrile and evidence for very high excited state yields from electron transfer reactions**. *J Phys Chem* 1979, **83**:1350–1357.

49. McCord P, Bard AJ: **Electrogenerated chemiluminescence. Part 54. Electrogenerated chemiluminescence of ruthenium(II) 4,4'-diphenyl-2,2'-bipyridine and ruthenium(II) 4,7-diphenyl-1,10-phenanthroline systems in aqueous and acetonitrile solutions**. *J Electroanal Chem* 1991, **318**:91–99.

50. Maness KM, Bartelt JE, Wightman RM: **Effects of solvent and ionic strength on the electrochemiluminescence of 9,10-diphenylanthracene**. *J Phys Chem* 1994, **98**:3993–3998.

51. Collinson MM, Wightman RM: **High-frequency generation of electrochemiluminescence at microelectrodes**. *Anal Chem* 1993, **65**:2576–2582.

52. Villani E, Sakanoue K, Einaga Y, Inagi S, Fiorani A: **Photophysics and electrochemistry of ruthenium complexes for electrogenerated chemiluminescence**. *J Electroanal Chem* 2022, **921**, 116677.

53. Miao W, Choi JP, Bard AJ: **Electrogenerated chemiluminescence 69: the Tris(2,2′-bipyridine)ruthenium(II), (Ru(bpy)32+)/tri-n-propylamine (TPrA) system revisited - a new route involving TPrA.+ cation radicals**. *J Am Chem Soc* 2002, **124**:14478–14485.

54. * Fu W, Zhou P, Guo W, Su B: **Imaging electrochemiluminescence layer to dissect concentration-dependent light intensity for accurate quantitative analysis**. *Adv Sens Energy Mater* 2022, **1**:1–7.
By means of ECL microscopy, the authors explored the thickness variation of the ECL emitting layer with the concentration ratio of $[Ru(bpy)_3]^{2+}$ to TPrA (cRu/cTPrA) within homogeneous ECL. Using carbon fiber as the working electrode, TEL was observed to grow with the increase of cRu/cTPrA remarkably.

55. ** Adsetts JR, Chu K, Hesari M, Ma J, Ding Z: **Absolute electrochemiluminescence efficiency quantification strategy exemplified with Ru(bpy)32+in the annihilation pathway**. *Anal Chem* 2021, **93**:11626–11633.
The authors proposed a novel framework for determining the absolute and instrumental- independent ECL efficiencies relative to $[Ru(bpy)_3]^{2+}$, regardless of whether the conditions are favorable for $[Ru(bpy)_3]^{2+}$ emissions or not.

56. ** Chu K, Adsetts JR, Ma J, Zhang C, Hesari M, Yang L, Ding Z: **Physical strategy to determine absolute electrochemiluminescence quantum efficiencies of coreactant systems using a photon-counting photomultiplier device**. *J Phys Chem C* 2021, **125**:22274–22282.
Here, the authors determine the absolute ECL-QE of the $[Ru(bpy)_3]^{2+}$/TPrA co-reactant ECL system for the first time, by exploiting a novel photon counting intrument. They report a 3-fold efficiency enhancement compared to that in annihilation pathway.

57. Yang L, Adsetts JR, Zhang R, Balónová B, Piqueras MT, Chu K, Zhang C, Zysman-Colman E, Blight BA, Ding Z: **Determining absolute electrochemiluminescence efficiencies of two iridium complexes**. *J Electroanal Chem* 2022, **906**, 115891.

58. Qin X, Yang L, Wang X, Patel D, Chu K, Kelland L, Adsetts JR, Zhang C, Workentin MS, Pagenkopf BL, Ding Z: **Correlating structures to electrochemiluminescence efficiencies of silole compounds in coreactant systems**. *Chemelectrochem* 2022, **9**, e202200605.

59. ** Adsetts JR, Chu K, Hesari M, Whitworth Z, Qin X, Zhan Z, Ding Z: **Absolute electrochemiluminescence quantum efficiency of Au nanoclusters by means of a spectroscopy charge-coupled device camera**. *J Phys Chem C* 2022, **126**:20155–20162.
The authors present an instrumentally and mathematically simpler method to determine ECL-QE using only a spectrometer coupled with a CCD camera. The accuracy of this new strategy is verified with the well-studied $[Ru(bpy)_3]^{2+}$ and is then exemplified with Au nanoclusters.

60. Ryer AD: *The light measurement handbook*. Peabody, MA: International Light Technologies; 1997, 01960.

61. ** Ding J, Zhou P, Su B: **Quantum efficiency of electrochemiluminescence generation by tris(2,2'-bipyridine)ruthenium(II) and tri-n-propylamine revisited from a kinetic reaction model**. *Chemelectrochem* 2022, **9**:91–99.
Taking the $[Ru(bpy)_3]^{2+}$/TPrA co-reactant system as an example, the authors evaluate the ECL-QE in terms of a kinetic reaction model. They use finite element simulations to examine the variation of electrochemical excitation efficiency with the electrode material, applied potential, concentration and distance from the electrode surface.

62. Rebeccani S, Wetzl C, Zamolo VA, Criado A, Valenti G, Paolucci F, Prato M: **Electrochemiluminescent immunoassay enhancement driven by carbon nanotubes**. *Chem Commun* 2021, **57**:9672–9675.

63. Yang X, Hang J, Qu W, Wang Y, Wang L, Zhou P, Ding H, Su B, Lei J, Guo W, Dai Z: **Gold microbeads enabled proximity electrochemiluminescence for highly sensitive and size-encoded multiplex immunoassays**. *J Am Chem Soc* 2023, **145**:16026–16036.

64. ** Zanut A, Fiorani A, Canola S, Saito T, Ziebart N, Rapino S, Rebeccani S, Barbon A, Irie T, Josel HP, Negri F, Marcaccio M, Windfuhr M, Imai K, Valenti G, Paolucci F: **Insights into the mechanism of coreactant electrochemiluminescence facilitating enhanced bioanalytical performance**. *Nat Commun* 2020, **11**.
The authors propose an innovative framework that exploit the TOF concept for assessing the emission efficiency of a single $[Ru(bpy)_3]^{2+}$ label in bead-based immunoassay, which represents the only existing method to date.